Jurnal Teknologi

Full Paper

# EXCELLENT REMOVAL COPPER PERFORMANCE BY $CO_XFE_{3-X}O_4$/ZNO/AC NANOCOMPOSITE

Falichal Abida Fi Ramadhani[a], Robi Kurniawan[a], ST. Ulfawanti Intan Subadra[a], Hari Wisodo[a], Nurul Hidayat[a], Markus Diantoro[a], Nandang Mufti[a,b], Ahmad Taufiq[a]*

[a]Department of Physics, Faculty of Mathematics and Natural Sciences, Universitas Negeri Malang, Indonesia
[b]Center of Advanced Materials for Renewable Energy, Universitas Negeri Malang, Indonesia

**Article history**
Received
*26 July 2024*
Received in revised form
*18 December 2024*
Accepted
*23 December 2024*
Published Online
*22 August 2025*

*Corresponding author
ahmad.taufiq.fmipa@um.ac.id

## Graphical abstract

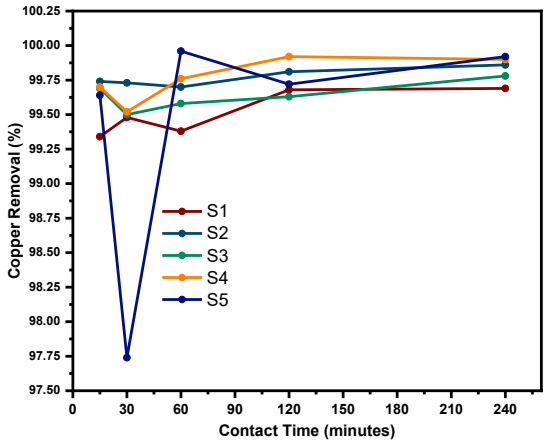


## Abstract

In recent years, the rapidly growing industry has also harmed aquatic life due to water pollution, especially heavy metal pollution. Herein, the $Co_xFe_{3-x}O_4$/ZnO/activated carbon (AC) nanocomposite was synthesized via the coprecipitation and sol–gel methods to apply as a copper adsorbent. X-ray diffractometry revealed the cubic spinel crystal structure of $Co_xFe_{3-x}O_4$ and the hexagonal wurtzite structure of ZnO. Examination under scanning electron microscopy depicted the morphology of the samples as comprising spheres, sheets, and chunks. The spherical nanoparticles exhibited an average particle size of 45.08–65.36 nm. Fourier transform infrared spectra confirmed the presence of all components within the nanocomposite, including $Co_xFe_{3-x}O_4$, ZnO, and AC. Analysis using a vibrating sample magnetometer indicated the superparamagnetic nature of the nanocomposite, 11.069–23.514 emu/g with magnetic saturation value. To assess the influence of Co composition, adsorption experiments were conducted with varying contact time intervals. Remarkably, these experiments demonstrated the copper removal efficiencies of samples S1-S4 was 9969%, 99.86%, 99.76% and 99.92%, respectively, while the best copper removal efficiency of 99.96% was achieved by sample S5, with 11.00 mg/g maximum adsorption capacity. Thus, the $Co_xFe_{3-x}O_4$/ZnO/AC nanocomposite demonstrates significant potential as a novel material for copper removal in adsorption applications.

Keywords: $Co_xFe_{3-x}O_4$/ZnO/AC, nanocomposite, iron sand, copper adsorbent

## 1.0 INTRODUCTION

In recent years, the transition to Industry 4.0 and the impending shift to Industry 5.0 have been witnessed globally, marked by rapid industrial development, including the mining sector. However, this accelerated growth has exacerbated water pollution [1]. Heavy metal contamination represents a significant portion of this pollution [2], posing a critical threat due to the toxicity, nondegradability, and bioaccumulation of heavy metals, endangering human health and environmental safety [3]. Particularly, copper pollution in river bodies has been recorded at 0.413 mg/L average concentration, surpassing government regulatory limits [4], whereas the standard for acceptable copper concentration in river water is recognized at 0.02 mg/L [5]. Consequently, effective waste management is crucial, especially before disposing waste in river bodies. The use of adsorption with adsorbent materials has been a favored approach owing to its easy synthesis process, cost-effectiveness, and high efficiency at low concentrations [6]. The widespread availability of adsorbent materials, such as carbon materials, polymers, zeolites, and nanomaterials, further promotes the application of this method [7].

Ferrite nanoparticles, especially cobalt ferrite ($Co_xFe_{3-x}O_4$), have garnered attention as promising adsorbents for copper metal [8]. Among various ferrite materials, $Co_xFe_{3-x}O_4$ is widely acknowledged as an adsorbent due to its chemical stability, mechanical strength, and high magnetization, which enables rapid accumulation after distribution in water [9], [10]. Additionally, $Co_xFe_{3-x}O_4$ offers the advantages of being easily separated from the contaminant and reusable under an external magnetic field, which has a positive environmental impact [11]. A study reported successful copper ion adsorption using $Co_xFe_{3-x}O_4$, achieving equilibrium within 300 min with removal efficiency of copper 99.5% [12]. However, $Co_xFe_{3-x}O_4$ nanoparticles tend to agglomerate in solution owing to magnetic bonds, impacting their adsorption efficacy and dispersion stability [13]. Thus, this study introduced ZnO into the composite system to enhance adsorption properties. ZnO offers a high surface area, porosity, antimicrobial activity, nontoxicity, simple synthesis, and various functional groups conducive to heavy metal adsorption [14–16]. Leiva *et al*. stated that ZnO nanoparticles removed copper ions with a maximum adsorption capacity of 47.5 mg/g and a removal efficiency of 98.4% [15]. Goyal *et al*. also observed that ZnO/$Fe_3O_4$ composites effectively removed copper ions over 480 min, with adsorption efficiency of 37.66% [17].

Furthermore, the $Co_xFe_{3-x}O_4$/ZnO nanocomposite adsorption performance can be enhanced by incorporating a highly porous material such as carbon. Activated carbon (AC) is an effective adsorbent for heavy metals in industrial wastewater, attributed to its expansive surface area, microporous structure, high surface reactivity, and superior adsorption qualities [18]. AC is known to be capable of adsorbing copper ions, with a maximal adsorption capacity of 57.39 mg/g within 120 min [19]. Another research revealed that the removal of copper using AC reached an equilibrium time 12 h with a removal efficiency 63% [20].

Therefore, in this work, the use of $Co_xFe_{3-x}O_4$/ZnO/AC nanocomposite as copper adsorbent is unique because it offers advantages in efficiency, cost-effectiveness, and good environmental impact, making it expected to be utilized as an alternative for wastewater treatment. Interestingly, the present study utilizes iron sand and coconut shells to produce $Co_xFe_{3-x}O_4$ for AC synthesis. Iron sand is a verified source for producing high-purity $Co_xFe_{3-x}O_4$ [21], while coconut shells were selected because of their advantageous natural structure and low ash content [22]. These natural precursors made $Co_xFe_{3-x}O_4$ and AC low-cost, because they are relativity abundant in nature and cheap [23]. Despite numerous studies on copper metal adsorption, research on the development of $Co_xFe_{3-x}O_4$/ZnO/AC nanocomposite as a copper adsorbent remains limited. Consequently, this investigation examines the impact of varying cobalt molar fractions on the structural characteristics, morphology, functional groups, and magnetic properties of nanocomposite. Furthermore, it explores their relationship with the adsorption efficiency of the nanocomposite in removing copper heavy metal.

## 2.0 METHODOLOGY

### 2.1 $Co_xFe_{3-x}O_4$/ZnO/AC Nanocomposite Synthesis

The materials utilized for synthesizing the $Co_xFe_{3-x}O_4$/ZnO/AC nanocomposite included iron sand, coconut shell, hydrochloric acid (HCl) 12M, cobalt (II) chloride hexahydrate ($CoCl_2.6H_2O$), ammonium hydroxide ($NH_4OH$) 6.5 M, zinc acetate dihydrate, sodium hydroxide (NaOH), copper sulfate ($CuSO_4$), deionized water, and distilled water. This study prepared $Co_xFe_{3-x}O_4$ with molar fractions of x = 0, 0.2, 0.4, 0.6, and 0.8 *via* the coprecipitation method, as delineated in a preceding study [24]. Initially, the iron sand was dissolved in HCl and stirred, forming an iron chloride solution. Subsequently, the iron chloride solution was combined with $CoCl_2.6H_2O$. The mixture was then titrated with 25 mL of $NH_4OH$ under stirring. Posttitration, the solution was repeatedly washed until the precipitate reached neutrality. The precipitate was then separated and dried at 100°C for 1 h. Concurrently, the synthesis of ZnO nanoparticles involved dissolving zinc acetate dihydrate in deionized water and reaction using NaOH, with the steps followed by our previous study [25].

The synthesis of coconut shell-based AC commenced with burning the coconut shell to charcoal, which was then crushed and calcinated at 400°C for 5 h. Thereafter, the $Co_xFe_{3-x}O_4$/ZnO/AC

nanocomposite was synthesized by dissolving $Co_xFe_{3-x}O_4$ in 25 mL distilled water and stirred for 1 h, then mixed with ZnO powder and stirred for an additional hour. Subsequently, coconut shell-based AC powder was added to the $Co_xFe_{3-x}O_4$/ZnO solution, stirred for 90 min, and dried at 100°C. Each sample of the $Co_xFe_{3-x}O_4$/ZnO/AC nanocomposite was labeled S1–S5, corresponding to the molar fraction variations of $x$ = 0, 0.2, 0.4, 0.6, and 0.8.

### 2.2 Characterization

X-ray diffractometry (XRD) characterization of the $Co_xFe_{3-x}O_4$/ZnO/AC nanocomposite was conducted using a PANanalytical X'Pert Cu–Ka radiation to determine its crystal structure. The functional groups were identified using Fourier transform infrared spectroscopy (FTIR) Merk Shimadzu IR Prestige 21. The surface morphology was examined under the scanning electron microscopy (SEM) Merk FEI-INSPECT-S50. The magnetic properties were characterized using vibrating sample magnetometry (VSM). For the adsorption experiments, 0.05 g of $Co_xFe_{3-x}O_4$/ZnO/AC nanocomposite was reacted with 25 mL of copper solution and stirred at varying contact durations of 15, 30, 60, 120, and 240 min. The solution and residue were then separated, and the filtrate was characterized using atomic absorption spectrophotometry (AAS). The adsorption capacity ($q_t$) and copper metal sorption efficiency (%) were calculated using Equations (1) and (2).

$$q_t = (C_0\text{-}C_t)/m\times V \quad (1)$$

$$\%\text{Adsorption} = (C_0\text{-}C_t)/\ C_0\times 100\% \quad (2)$$

where ($q_t$) denotes the adsorption capacity, $C_o$ represents initial solution concentrations ($mg$/L), $C_t$ residual solution concentrations ($mg$/L), m shows the adsorbent mass ($g$), and $V$ is the volume of solutions (liter).

## 3.0 RESULTS AND DISCUSSION

The XRD pattern of all $Co_xFe_{3-x}O_4$/ZnO/AC nanocomposite samples is presented in Figure 1, suggesting that the diffraction peaks correspond to $Fe_3O_4$ with cubic spinel inverse structure (AMCSD No. 0002402) and ZnO with the hexagonal wurtzite structure of (AMCSD No. 0011555). In addition, Figure 1 (a) depicts the $Co_xFe_{3-x}O_4$ diffraction peaks from S1 sample observed at 2θ 30.29°; 35.68°; 43.37°; 53.82°; 57.22°; 63.02°, which successively occupy the hkl planes of (2 2 0), (3 1 1), (4 0 0), (4 2 2), (5 1 1), and (4 4 0), respectively. Moreover, the diffraction peak of ZnO was observed at 2θ 31.79°; 34.48°; 36.28°; 47.60°; 56.63°; 62.96°, representing the hkl planes of (0 1 0), (0 0 2), (0 1 1), (0 1 2), (1 1 0), and (0 1 3). Notably, the peak shifts toward a lower angle at the Bragg plane (3 1 1) (Figure 1 (b)) are attributable to the increase in the interplane distance (d) in the spinel structure [26]. This is consistent with the increasing lattice parameter of $Co_xFe_{3-x}O_4$, following the accelerated molar fraction of Co from 8.358 to 8.376 Å. This increase in lattice parameter correlates with the presence of the $Co^{2+}$ ion (74 pm), successfully replacing parts of the $Fe^{3+}$ ion (69 pm) in tetrahedral and octahedral sites [27]. This enhanced lattice parameter aligns with the Vegard Law [28]. Moreover, the lattice parameter of ZnO tends to be constant, ranging from $a = b$ = 3.250–3.255 Å and c = 5.202–5.214 Å. The crystallite size of $Co_xFe_{3-x}O_4$ and ZnO ranges between 9.94–11.77 nm, whereas their lattice parameters ($a = b = c$) range 8.358–8.376 Å (Table 1).

$$r_A = x.r_{(Co^{2+})} + (1-x).r_{(Fe^{3+})} \quad (3)$$

$$r_B = \frac{1}{2}\left[1.r_{(Fe^{2+})} + (1-x).r_{(Fe^{3+})} + (x).r_{(Co^{2+})}\right] \quad (4)$$

where $r_A$ denotes the ionic radius at the tetrahedral site, $r_B$ indicates the ionic radius at the octahedral site, and x represents the cation concentration. Furthermore, the values of tetrahedral ($r_A$) and octahedral ($r_B$) ionic radii are calculated from Equations (3–4). Based on Table 2, it's known that both the ionic radii increase with the higher molar fraction of Co. Therefore, the Co ions successfully successfully replace Fe ions in tetrahedral and octahedral sites of $Fe_3O_4$ with cubic spinel structure.

**Table 1** Crystallite Size and Lattice Parameters of $Co_xFe_{3-x}O_4$/ZnO/AC Nanocomposite

| Sample | Crystallite size (nm) | | Lattice Parameter (Å) | | |
|---|---|---|---|---|---|
| | $Co_xFe_{3-x}O_4$ | ZnO | $Co_xFe_{3-x}O_4$ | ZnO | |
| | | | $a = b = c$ | $a = b$ | $c$ |
| S1 | 9.94 | 18.03 | 8.358 | 3.250 | 5.210 |
| S2 | 10.59 | 19.92 | 8.364 | 3.251 | 5.211 |
| S3 | 11.28 | 19.95 | 8.366 | 3.253 | 5.212 |
| S4 | 11.32 | 20.43 | 8.374 | 3.254 | 5.213 |
| S5 | 11.77 | 21.38 | 8.376 | 3.255 | 5.214 |

**Table 2** Ionic Radius of $Co_xFe_{3-x}O_4$ Nanoparticle

| Sample | rA (Å) | rB (Å) |
|---|---|---|
| S1 | 0.64 | 0.69 |
| S2 | 0.66 | 0.70 |
| S3 | 0.68 | 0.71 |
| S4 | 0.70 | 0.72 |
| S5 | 0.77 | 0.73 |

Figure 2 illustrates the surface morphology of the $Co_xFe_{3-x}O_4$/ZnO/AC nanocomposite, revealing three distinct morphologies: spherical, sheet, and chunks. The analysis of the spherical yielded an average particle size of 45.08–65.36 nm (Figure 2). This range aligns with previous reports of $Fe_3O_4$/ZnO particle sizes between 48 and 67 nm [29] Notably, the observed particle size is larger than the crystal size indicated by XRD analysis, possibly due to the agglomeration originating from the strong interactions between particles due to van der Waals forces and magnetic dipolar interactions [30].

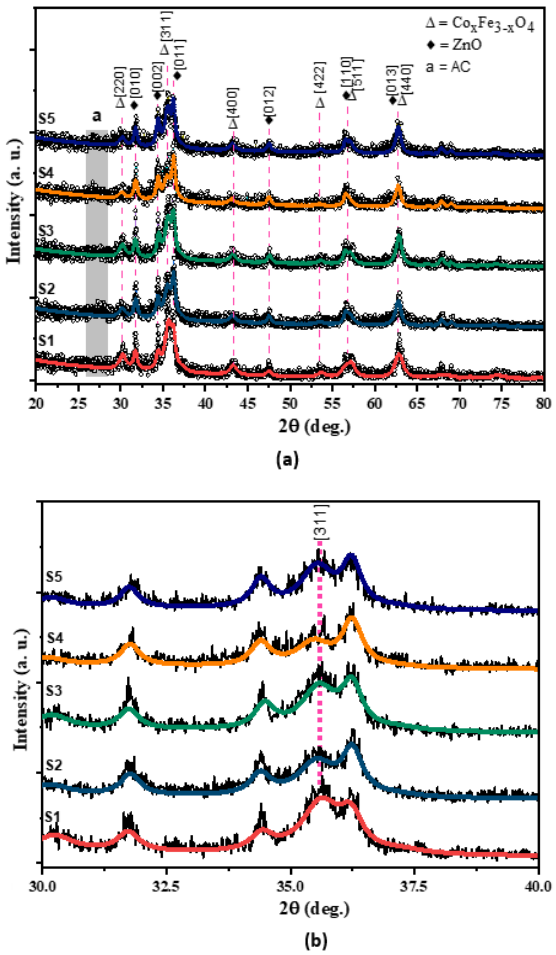


**Figure 1** Diffraction Pattern of $Co_xFe_{3-x}O_4$/ZnO/AC Nanocomposite (a) and Magnification of Diffraction pattern on the hkl plane (311) (b)

The FTIR characterization of the functional groups of the $Co_xFe_{3-x}O_4$/ZnO/AC nanocomposite is shown in Figure 3. The figure reveals the presence of O–H stretching of the carboxyl functional group at 3,500 $cm^{-1}$, indicative of residual water in the sample [31]. The vibration peaks of the C–H bond were observed at 2,884 and 2,831 $cm^{-1}$, consistent with previous findings that identified C–H bond vibrations at 2,921 and 2,852 $cm^{-1}$ [32]. Additionally, the vibration bonds of C=O, C=C, and C–O were detected at 2,314, 1,640, and 1,503 $cm^{-1}$, respectively [33, 34], with peaks of C=O bond detected at 1,390 $cm^{-1}$ [33]. Furthermore, the vibration of the C–$H_3$ bond was identified at 1,360 $cm^{-1}$. The C–H bond out-of-plane bending was observed at 990 $cm^{-1}$, aligning with another study that reported similar vibrations at 866–899 $cm^{-1}$ [35].

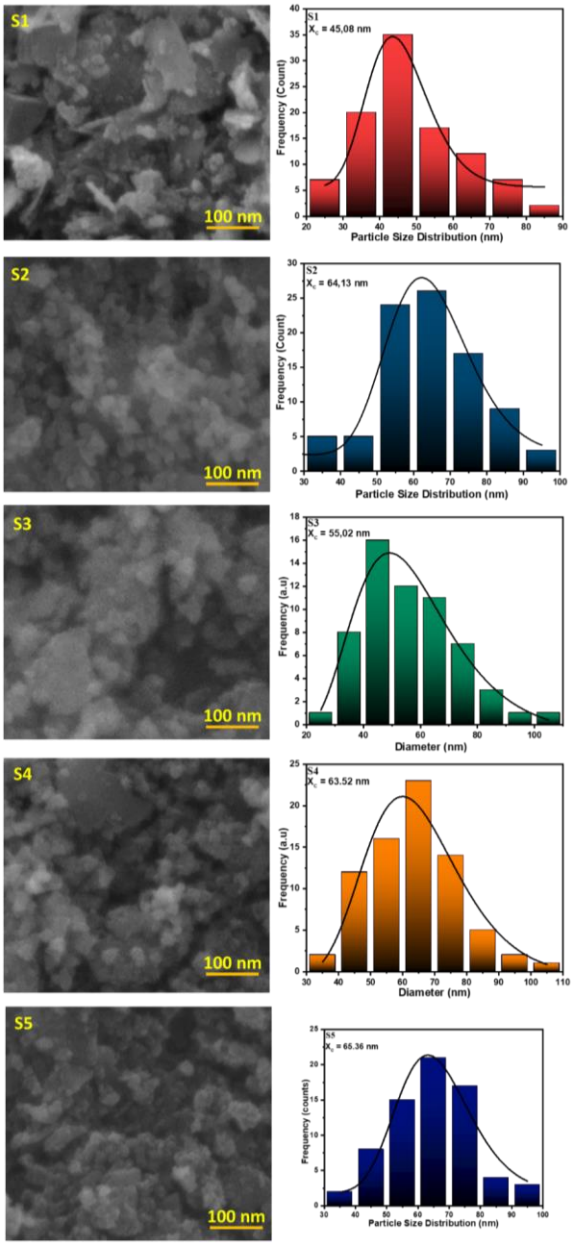


**Figure 2** The Size Distribution Histogram of $Co_xFe_{3-x}O_4$/ZnO/AC Nanocomposite

Furthermore, two vibration peaks were observed at 698–688 and 418–415 $cm^{-1}$, representing the metal oxide (Fe–O) bond at tetrahedral and octahedral sites. Another research reported the emergence of Fe–O vibration at 589 and 417 $cm^{-1}$ [36]. In this case, the blue shift phenomenon occurs and the FTIR absorption shifts to high wavenumbers owing to a reduction in particle size, enhancing the forces on the surface of the nanoparticles [37]. Moreover, the Zn–O vibration bond was observed at 514 $cm^{-1}$. The appearance of this Zn–O vibration has been confirmed by a study reporting the vibration at <580 $cm^{-1}$ [38].

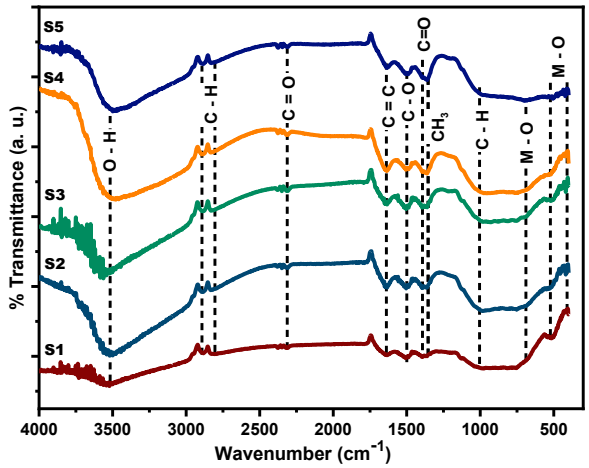


**Figure 3** FTIR Spectra of $Co_xFe_{3-x}O_4$/ZnO/AC Nanocomposite

The magnetic properties of the $Co_xFe_{3-x}O_4$/ZnO/AC nanocomposite were evaluated using VSM, with the hysteresis curves (Figure 4). These curves exhibit an S-shape, characterized by remanent magnetization ($M_r$) and coercivity ($H_c$) values that are negligible, confirming the superparamagnetic nature of all samples. This superparamagnetism is attributed to the reduced particle size and increased surface area [39]. Further analysis of the M–H curve using the Langevin method with susceptibility [25] revealed a decrease in magnetic saturation (Ms) with an increase in Co dopant, ranging from 23.514 to 11.069 emu/g. The comprehensive analysis is detailed in Table 3. The reduction in saturation magnetization is ascribed to the successful substitution of $Co^{2+}$ for $Fe^{3+}$ ions in the tetrahedral (A) and octahedral (B) sites of the $Co_xFe_{3-x}O_4$ system (Equation (5)). The introduction of $Co2^{+}$ into these sites reduces the magnetic moment, given that the magnetic moment of $Co^{2+}$ (3 μB) is lower than that of $Fe^{3+}$ (5 μB) and $Fe^{2+}$ (4 μB) [40]. Additionally, the decline in saturation magnetization may be linked to an increase in particle size distribution with higher Co doping. This correlation is consistent with previous findings that magnetization values decrease with increased particle size, a result of heat-induced redistribution of Fe ions [41].

$$(Co_{1-x}Fe_x)_A\,(Co_xFe_{2-x})_B \quad (5)$$

**Table 3** Saturation Magnetization of $Co_xFe_{3-x}O_4$/ZnO/AC Nanocomposite

| Sample | Ms (emu/g) | Mr (emu/g) | Hc (T) | χ |
|---|---|---|---|---|
| S1 | 23.514 | 0.009 | 0.041 | 0.841 |
| S2 | 14.796 | 0.010 | 0.046 | 0.860 |
| S3 | 22.729 | 0.011 | 0.052 | 0.805 |
| S4 | 11.069 | 0.004 | 0.058 | 0.891 |
| S5 | 18.468 | 0.019 | 0.071 | 0.925 |

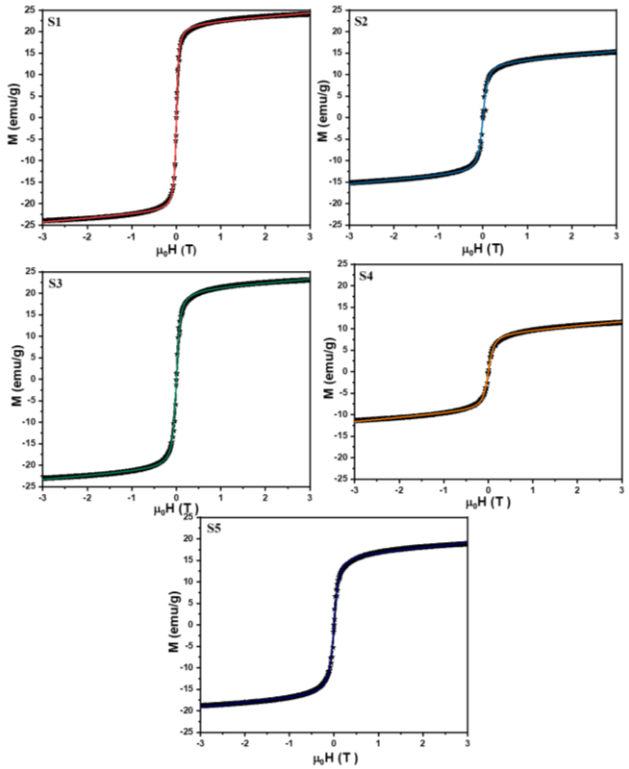


**Figure 4** Hysteresis Curve of $Co_xFe_{3-x}O_4$/ZnO/AC Nanocomposite

The copper metal uptake was assessed *via* batch adsorption experiments, where the metal uptake was examined over varying contact times, 15–240 min, starting with an initial copper concentration of 22.02 mg/L. Figure 5 presents these observations, demonstrating that the $Co_xFe_{3-x}O_4$/ZnO/AC nanocomposite is capable of removing copper metal with an efficiency of up to 99% within 15 min of contact. This efficiency remains relatively constant in subsequent intervals. Notably, there is no significant change in metal removal percentage as contact time extends from 15 (S1 = 99.3%) to 240 min (S2 = 99.6%). These results suggest that copper uptake reaches equilibrium after 15 min of contact time. The maximal adsorption capacity observed for samples S1–S3 at 240 min of contact time is 10.978, 10.996, and 10.987 mg/g, with efficiencies of 99.69%, 99.86%, and 99.78%, respectively. Conversely, samples S4 and S5 demonstrate maximum adsorption capacities of 11.002 and 11.006 mg/g at contact times of 120 and 60 min, respectively, with an efficiency of 99.92%. These analytical results are consolidated in Table 4. Accordingly, sample S5 exhibits the highest copper metal removal efficiency and capacity, identifying 60 min as the optimal contact period. During adsorption, interactions and collisions occur between metal ions and the adsorbent. Thus, an increase in contact time can enhance interactions, potentially disrupting molecular bonds and providing active sites for the adsorption of metal ions [42].

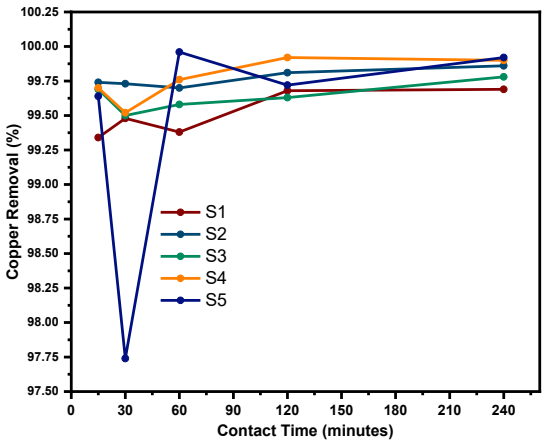


**Figure 5** Curve of The Effect of Contact Time on Copper Removal Efficiency by $Co_xFe_{3-x}O_4$/ZnO/AC Nanocomposite

Adsorption is defined as the transfer of a substance (adsorbate) from a gaseous or liquid phase to a solid or liquid phase (substrate), leading to the formation of a thin molecular layer *via* physical or chemical interactions [43]. Metal ion absorption is typically categorized into physical (physisorption) and chemical (chemisorption) adsorptions, based on the nature of interaction between the adsorbent and adsorbate molecules [44]. Physisorption involves weak electrostatic interactions such as van der Waals interactions, dipole–dipole forces, and London forces. In contrast, chemisorption includes the covalent bonding of adsorbates to the substrate through transfer steps, with interactions typically being twice as strong as those in physisorption [45]. The adsorption process typically includes several stages. The initial stage, external mass transfer, involves the movement of the adsorbate to the exterior of the adsorbent, followed by intraparticle diffusion, where adsorbate molecules diffuse to the surface and pores of the adsorbent. Subsequently, the adsorbate molecules adhere to the adsorbent surface at active adsorption sites [46, 47].

## 4.0 CONCLUSION

The $Co_xFe_{3-x}O_4$/ZnO/AC nanocomposite synthesis has been confirmed through the identification of two distinct diffraction peak phases: the $Fe_3O_4$ phase with a *cubic inverse spinel structure* and the ZnO phase with a hexagonal wurtzite structure. Observations indicate an increase in the crystallite size of $Co_xFe_{3-x}O_4$ and ZnO with high $Co^{2+}$ ion concentrations. Moreover, the substitution of $Co^{2+}$ ions in $Fe_3O_4$ is evidenced by increasing lattice parameter, as indicated by the shift of the $Fe_3O_4$ diffraction peak to a small angle. SEM analysis of the $Co_xFe_{3-x}O_4$/ZnO/AC nanocomposite reveals morphologies of spherical, sheet, and chunks, with an average particle size of 45.08–65.36 nm. The FTIR test results identified the presence of Zn–O, Fe–O (octahedral), and Fe–O (tetrahedral) bond functional groups at wave numbers 441, 415, and 506 $cm^{-1}$, respectively. Additionally, the C–O–C bond, characteristic of the presence of AC, was observed at 1,181 $cm^{-1}$. The magnetic properties of the nanocomposite are identified as superparamagnetic, with an 11.069–23.514 emu/g magnetic saturation value. AAS characterization reveals that the percentage of copper metal removal does not significantly vary with increased contact time or $Co^{2+}$ molar fraction. Ultimately, copper uptake reaches equilibrium at a contact time of 15 min, achieving 99% adsorption.

## Acknowledgement

This research was funded by DRPTM RI through the PPS/PTM grant scheme for AT with contract number 3.4.130/UN32.20.1/LT/2023.

## Conflicts of Interest

The authors declare that there is no conflict of interest regarding the publication of this paper.

## References

[1] Bai, Q., Huang, C., Ma, S., Gong, B., Ou, J. 2023. Rapid Adsorption and Detection of Copper Ions in Water by Dual-functional Ion-imprinted Polymers Doping with Carbon Dots. *Sep Purif Technol*. 315: 123666. Doi: 10.1016/j.seppur.2023.123666.

[2] Shahrashoub, M., Bakhtiari, S. 2021. The Efficiency of Activated Carbon/magnetite Nanoparticles Composites in Copper Removal: Industrial Waste Recovery, Green Synthesis, Characterization, and Adsorption-desorption Studies. *Microporous Mesoporous Mater*. 311: 110692. Doi: 10.1016/j.micromeso.2020.110692.

[3] Deng, H., Li, Q., Huang, M., Li, A., Zhang, J., Li, Y., *et al*. 2020. Removal of Zn(II), Mn(II) and Cu(II) by Adsorption Onto Banana Stalk Biochar: Adsorption Process and Mechanisms. *Water Sci Technol*. 82(12): 2962–2974. Doi: 10.2166/wst.2020.543.

[4] Berlian, A. I., Raharjo, M., Dewanti, N. A. Y. 2023. Analysis of Water Quality and Environmental Health Risks of Copper (Cu) to Fish in Progo River Magelang Regency. *IAIP Conference Proceedings.* Doi:10.1063/5.0126500

[5] Government Regulation of the Republic of Indonesia Number 22 of 2021 concerning the Implementation of Environmental Protection and Management (2021), https://peraturan.bpk.go.id/Details/161852/pp-no-22-tahun-2021.

[6] Alizadeh, M., Peighambardoust, S. J., Foroutan, R., Azimi, H., Ramavandi, B. 2022. Surface Magnetization of Hydrolyzed Luffa Cylindrica Biowaste with Cobalt Ferrite Nanoparticles for Facile Ni2+ Removal from Wastewater. *Environ Res*. 212: 113242. Doi: 10.1016/j.envres.2022.113242.

[7] Ai, L., Li, M., Li, L. 2011. Adsorption of Methylene Blue from Aqueous Solution with Activated Carbon/Cobalt Ferrite/Alginate Composite Beads: Kinetics, Isotherms, and Thermodynamics. *J Chem Eng Data*. 56(8): 3475–3483. Doi:10.1021/je200536h.

[8] Tatarchuk, T., Mironyuk, I., Kotsyubynsky, V., Shyichuk, A., Myslin, M., Boychuk, V. 2020. Structure, Morphology and Adsorption Properties of Titania Shell Immobilized onto

Cobalt Ferrite Nanoparticle Core. *J Mol Liq*. 297: 111757. Doi: 10.1016/j.molliq.2019.111757.
[9] Khoshkerdar, I., Esmaeili, H. 2019. Adsorption of Cr (III) and Cd (II) Ions using Mesoporous Cobalt-Ferrite Nanocomposite from Synthetic Wastewater. *Acta Chim Slov*. 15: 208–216. Doi:10.17344/acsi.2018.4795.
[10] Tatarchuk, T., Shyichuk, A., Sojka, Z., Gryboś, J., Naushad, Mu, Kotsyubynsky, V., *et al*. 2021. Green Synthesis, Structure, Cations Distribution and Bonding Characteristics of Superparamagnetic Cobalt-zinc Ferrites Nanoparticles for Pb(II) Adsorption and Magnetic Hyperthermia Applications. *J Mol Liq*. 328: 115375. Doi: 10.1016/j.molliq.2021.115375
[11] Vamvakidis, K., Kostitsi, T. M., Makridis, A., Dendrinou-Samara, C. 2020. Diverse Surface Chemistry of Cobalt Ferrite Nanoparticles to Optimize Copper(II) Removal from Aqueous Media. *Materials*. 13(7): 1537. Doi: 10.3390/ma13071537.
[12] Asri, N. S., Nurdila, F. A., Kato, T., Iwata, S., Suharyadi, E. 2018. Removal Study of Cu(II), Fe(II) and Ni(II) Ions from Wastewater using Polymer-Coated Cobalt Ferrite ($CoFe_2O_4$) Magnetic Nanoparticles Adsorbent. *J Phys Conf Ser*. 1091: 012016. Doi: 10.1088/1742-6596/1091/1/012016.
[13] Wu, X., Wang, W., Li, F., Khaimanov, S., Tsidaeva, N., Lahoubi, M. 2016. PEG-assisted Hydrothermal Synthesis of $CoFe_2O_4$ Nanoparticles with Enhanced Selective Adsorption Properties for Different Dyes. *Appl Surf Sci*. 389: 1003–1011. Doi: 10.1016/j.apsusc.2016.08.053.
[14] Shaba, E. Y., Jacob, J. O., Tijani, J. O., Suleiman, M. A. T. 2021. A Critical Review of Synthesis Parameters Affecting the Properties of Zinc Oxide Nanoparticle and its Application in Wastewater Treatment. *Appl Water Sci*. 11(2): 48. Doi:10.1007/s13201-021-01370-z.
[15] Leiva, E., Tapia, C., Rodríguez, C. 2021. Highly Efficient Removal of Cu(II) Ions from Acidic Aqueous Solution using ZnO Nanoparticles as Nano-Adsorbents. *Water*. 13(21): 2960. Doi:10.3390/w13212960.
[16] Ahmad, S. Z. N., Salleh, W. N. W., Yusof, N., Mohd Yusop, M. Z., Hamdan, R., Awang, N. A., *et al*. 2021. Pb(II) Removal and Its Adsorption from Aqueous Solution using Zinc Oxide/graphene Oxide Composite. *Chem Eng Commun*. 208(5): 646–660. Doi: 10.1080/00986445.2020.1715957.
[17] Goyal, P., Chakraborty, S., Misra, S. K. 2018. Multifunctional $Fe_3O_4$-ZnO Nanocomposites for Environmental Remediation Applications. *Environ Nanotechnol Monit Manag*. 10: 28–35. Doi: 10.1016/j.enmm.2018.03.003.
[18] Islam, M. S., Ang, B. C., Gharehkhani, S., Afifi, A. B. M. 2016. Adsorption Capability of Activated Carbon Synthesized from Coconut Shell. *Carbon Lett*. 20: 1–9. Doi: 10.5714/CL.2016.20.001.
[19] Kali, A., Amar, A., Loulidi, I., Jabri, M., Hadey, C., Lgaz, H., *et al*. 2022. Characterization and Adsorption Capacity of Four Low-cost Adsorbents based on Coconut, Almond, Walnut, and Peanut Shells for Copper Removal. *Biomass Convers Biorefinery*. 14: 3655–3666. Doi:10.1007/s13399-022-02564-4.
[20] Qin, Q., Wu, X., Chen, L., Jiang, Z., Xu, Y. 2018. Simultaneous Removal of Tetracycline and Cu(II) by Adsorption and Coadsorption Using Oxidized Activated Carbon. *RSC Adv*. 8(4): 1744–1752. Doi:10.1039/C7RA12402C.
[21] Yahya, M. M. A., Subadra, StUl, Saputro, R. E., Taufiq, A. Yogihati, C. I., Sunaryono, *et al*. 2023. Investigation of the Optical, Magnetic, and Radar Absorption Characteristics of $CoxFe_{3-x}O_4$/ZnO/graphite Nanocomposites. *Mater Sci Semicond Process*. 165: 107683. Doi: 10.1016/j.mssp.2023.107683.
[22] Adebayo, A., 2017. Removal of Heavy Metals from Petroleum Refinery Effluent using Coconut Shell-based Activated Carbon. *Card Int J Eng Emerg Sci Discov*. 2: 102–117.
[23] Yuliantika, D., Taufiq, A., Hidayat, A., Sunaryono, Hidayat, N, Soontaranon S. 2019. Exploring Structural Properties of Cobalt Ferrite Nanoparticles from Natural Sand. *IOP Conf Ser Mater Sci Eng*. 515: 012047. Doi: 10.1088/1757-899X/515/1/012047.
[24] Yuliantika, D., Taufiq, A., Hidayat, A., Sunaryono, Hidayat N., Soontaranon, S. 2019. Exploring Structural Properties of Cobalt Ferrite Nanoparticles from Natural Sand. *IOP Conf Ser Mater Sci Eng*. 515: 012047. Doi:10.1088/1757-899X/515/1/012047.
[25] Subadra, SUl, Taufiq, A., Sunaryono, S., Hidayat, A., Mufti, N., Susanto, H., *et al*. 2022. Synthesis and Characterisation of $Fe_3O_4$/MWCNT/ZnO Nanocomposites Covered by a Soft Template as a New Antibacterial Agent. *Adv Nat Sci Nanosci Nanotechnol*. 13(3): 035010. Doi:10.1088/2043-6262/ac8de8.
[26] H. Phong, L. T., H. Manh, D., H. Nam, P., D. Lam, V., X. Khuyen, B., S. Tung, B., *et al*. 2022. Structural, Magnetic and Hyperthermia Properties and Their Correlation in Cobalt-doped Magnetite Nanoparticles. *RSC Adv*. 12(2): 698–707. Doi:10.1039/D1RA07407E.
[27] Kumar, P., Pathak, S., Singh, A., Kuldeep, Khanduri, H., Wang, X., *et al*. 2021. Optimization of Cobalt Concentration for Improved Magnetic Characteristics and Stability of $CoxFe_{3-x}O_4$ Mixed Ferrite Nanomagnetic Fluids. *Mater Chem Phys*. 265: 124476. Doi: 10.1016/j.matchemphys.2021.124476.
[28] Vegard L. Die Konstitution der Mischkristalle und die Raumfüllung der Atome. 1921. *Z Für Phys*. 5(1): 17–26. Doi: 10.1007/BF01349680.
[29] Taufiq, A., Ulya, H. N., Yogihati, C. I., Sunaryono, Hidayat, N., Mufti, N., *et al*. 2020. Effects of ZnO Nanoparticles on the Antifungal Performance of $Fe_3O_4$/ZnO Nanocomposites Prepared from Natural Sand. *Adv Nat Sci Nanosci Nanotechnol*. 11(4): 045004. Doi: 10.1088/2043-6254/abb8c6.
[30] Shen, W., Ren, B., Cai, K., Song, Y. Fei, Wang, W. 2019. Synthesis of Nonstoichiometric Co0.8Fe2.2O4/reduced Graphene Oxide (rGO) Nanocomposites and Their Excellent Electromagnetic Wave Absorption Property. *J Alloys Compd*. 774: 997–1008. Doi: 10.1016/j.jallcom.2018.09.361.
[31] Golabiazar, R., Omar, Z. A., Ahmad, R. N., Hasan, S. A., Sajadi, S. M. 2020. Synthesis and Characterization of Antibacterial Magnetite-activated Carbon Nanoparticles. *J Chem Res*. 44(1–2):80–87. Doi: 10.1177/1747519819883884.
[32] Ramya V., Murugan D., Lajapathirai C., Sivasamy A. 2018. Activated Carbon (prepared from secondary sludge biomass) Supported Semiconductor Zinc Oxide Nanocomposite Photocatalyst for Reduction of Cr(VI) under Visible Light Irradiation. *J Environ Chem Eng*. 6(6): 7327–7337. Doi: 10.1016/j.jece.2018.08.055.
[33] Yadav, V. K., Ali, D., Khan, S. H., Gnanamoorthy, G., Choudhary, N., Yadav, K. K., *et al*. 2020. Synthesis and Characterization of Amorphous Iron Oxide Nanoparticles by the Sonochemical Method and Their Application for the Remediation of Heavy Metals from Wastewater. *Nanomaterials*. 10(8): 1551. Doi: 10.3390/nano10081551.
[34] Ali, O. I., Zaki, E. R., Abdalla, M. S., Ahmed, S. M. 2023. Mesoporous Ag-functionalized Magnetic Activated Carbon-based Agro-waste for Efficient Removal of Pb(II), Cd(II), and Microorganisms from Wastewater. *Environ Sci Pollut Res*. 30(18): 53548–53565. Doi: 10.1007/s11356-023-26000-w.
[35] Yahya, MohMA. 2020. Pengaruh Substitusi Co terhadap Struktur, Gugus Fungsi, dan Sifat Optik Nanokomposit $CoxFe_{3-x}O_4$/Grafit/ZnO. http://repository.um.ac.id/id/eprint/148596.
[36] Intan Subadra STU, Sutiami, R., Taufiq, A., Diantoro, M., Sunaryono, Arif, *et al.* 2019. Preparation and Characterization of Magnetite Nanoparticles Combined with Polyaniline and Activated Carbon. *IOP Conf Ser Earth*

*Environ Sci*. 276(1): 012041. Doi: 10.1088/1755-1315/276/1/012041.

[37] Taufiq, A., Saputro, R. E., Yuliantika, D., Sunaryono, S., Diantoro, M., Hidayat, A., *et al*. 2020. Excellent Antimicrobial Performance of Co-doped Magnetite Double-Layered Ferrofluids Fabricated from Natural Sand. *J King Saud Univ - Sci*. 32(7): 3032–3038. Doi: 10.1016/j.jksus.2020.08.009.

[38] Chandel, N., Sharma, K., Sudhaik, A., Raizada, P., Hosseini-Bandegharaei, A., Thakur, V. K., *et al*. 2020. Magnetically Separable ZnO/$ZnFe_2O_4$ and ZnO/$CoFe_2O_4$ Photocatalysts Supported onto Nitrogen Doped Graphene for Photocatalytic Degradation of Toxic Dyes. *Arab J Chem*. 13(2): 4324–4340. Doi: 10.1016/j.arabjc.2019.08.005.

[39] Mohammadi, Z., Attaran, N., Sazgarnia, A., Shaegh, S. A. M., Montazerabadi, A. 2020. Superparamagnetic Cobalt Ferrite Nanoparticles as $T_2$ Contrast Agent in MRI: In vitro Study. *IET Nanobiotechnol*. 14(5): 396–404. Doi: 10.1049/iet-nbt.2019.0210

[40] Yasemian, A. R., Kashi, M. A., Ramazani, A. 2020. Exploring the Effect of Co Concentration on Magnetic Hyperthermia Properties of $CoxFe_{3-x}O_4$ Nanoparticles. *Mater Res Express*. 7(1): 016113.

[41] Mukadam, M. D., Yusuf, S. M., Sharma, P., Kulshreshtha, S. K. 2004. Particle Size-dependent Magnetic Properties of γ-$Fe_2O_3$ Nanoparticles. *J Magn Magn Mater*. 272–276: 1401–1403. Doi:10.1016/j.jmmm.2003.12.139.

[42] Asri, N. S., Nurdila, F. A., Kato, T., Iwata, S., Suharyadi, E. 2018. Removal Sudy of Cu(II), Fe(II) and Ni(II) Ions from Wastewater Using Polymer-coated Cobalt Ferrite ($CoFe_2O_4$ ) Magnetic Nanoparticles Adsorbent. *J Phys Conf Ser*. 1091: 012016. Doi:10.1088/1742-6596/1091/1/012016.

[43] Dev, V. V., Nair, K. K., Baburaj, G., Krishnan, K. A. 2022. Pushing the Boundaries of Heavy Metal Adsorption: A Commentary on Strategies to Improve Adsorption Efficiency and Modulate Process Mechanisms. *Colloid Interface Sci Commun*. 49: 100626. Doi: 10.1016/j.colcom.2022.100626.

[44] Ray, S. S., Gusain, R., Kumar, N. 2020. Adsorption in the Context of Water Purification. *Carbon Nanomaterial-Based Adsorbents for Water Purification*. 67–100. Doi: 10.1016/B978-0-12-821959-1.00004-0.

[45] Sims, R. A., Harmer, S. L., Quinton, J. S. 2019. The Role of Physisorption and Chemisorption in the Oscillatory Adsorption of Organosilanes on Aluminium Oxide. *Polymers*. 11(3): 410. Doi:10.3390/polym11030410.

[46] Weyrich, J. N., Mason, J. R., Bazilevskaya, E. A., Yang, H. 2023. Understanding the Mechanism for Adsorption of Pb(II) Ions by Cu-BTC Metal–Organic Frameworks. *Molecules*. 28(14): 5443. Doi:10.3390/molecules28145443.

[47] Marzbali, M. H., Esmaieli, M. 2017. Fixed Bed Adsorption of Tetracycline on a Mesoporous Activated Carbon: Experimental Study and Neuro-fuzzy Modeling. *J Appl Res Technol JART*. 15(5): 454–463. Doi:10.1016/j.jart.2017.05.003.